Electronic Supplementary Material (ESI) for Journal of Materials Chemistry A.

Supporting Information

Core–shell Cu_2S:NiS_2@C Hybrid Nanostructure Derived from a Metal–Organic Framework with Graphene Oxide for Photocatalytic Synthesis of N-substituted Derivatives

Mohammad Yusuf[a], Shamim Ahmed Hira[a], Hyeonhan Lim[a], Sehwan Song[b], Sungkyun Park[b], Kang Hyun Park[a,*]

[a]*Department of Chemistry, Chemistry Institute for Functional Materials, Pusan National University, Busan, 46241, Republic of Korea*
[b]*Department of Physics, Pusan National University, Busan 46241, Republic of Korea*

E-mail: chemistry@pusan.ac.kr

Supplementary Figures

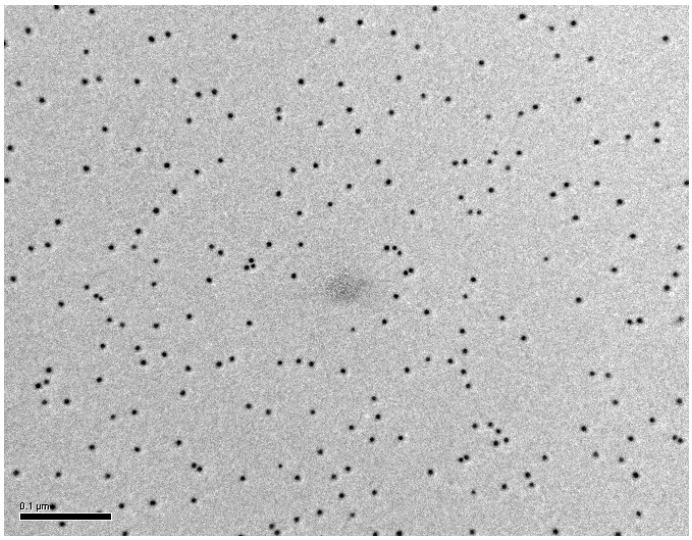

Figure S1. The seeding of the Cu:Ni-BTEC by reflux condition.

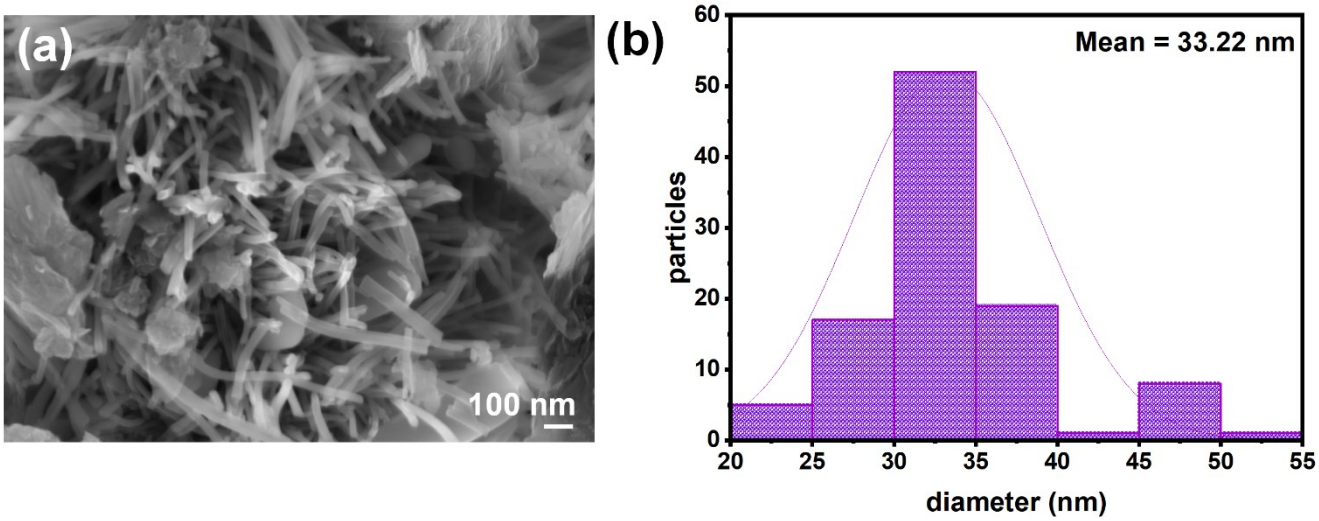

Figure S2. (a) SEM images of Cu:Ni-BTEC/GO and (b) histogram distribution diameter of Cu:Ni-BTEC/GO.

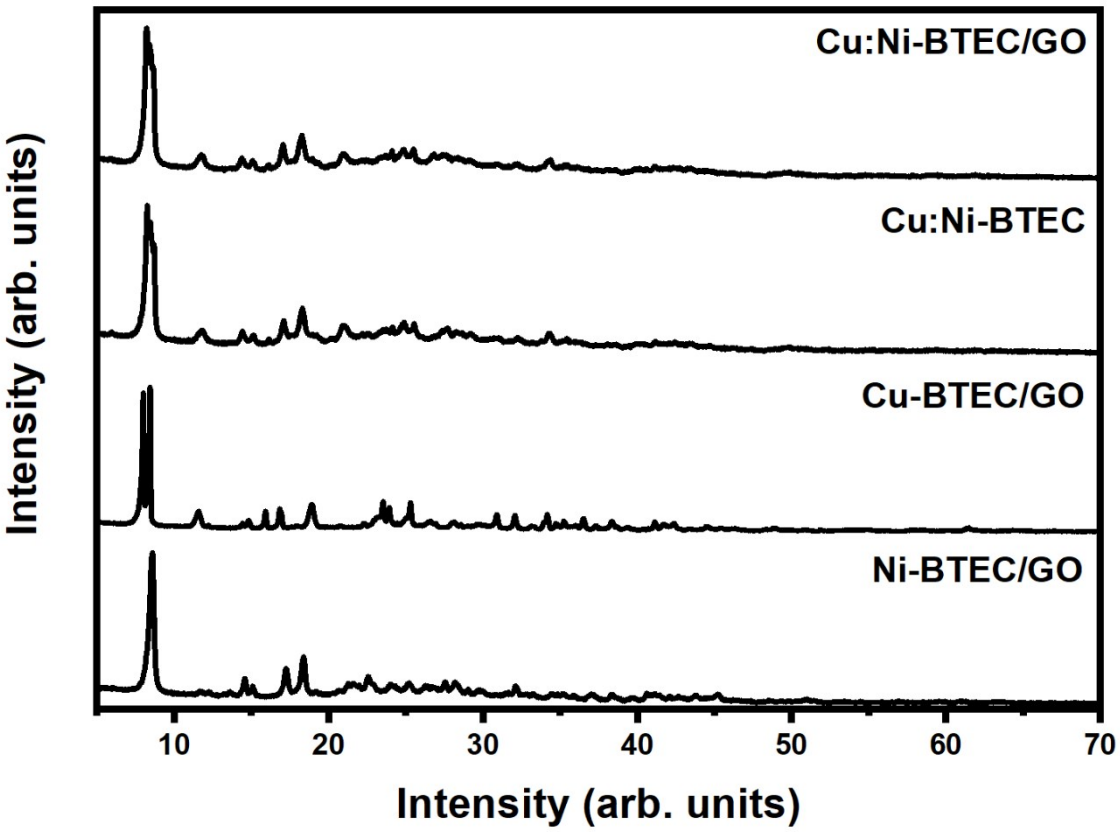

Figure. S3. XRD pattern of various Cu:Ni-BTEC/GO

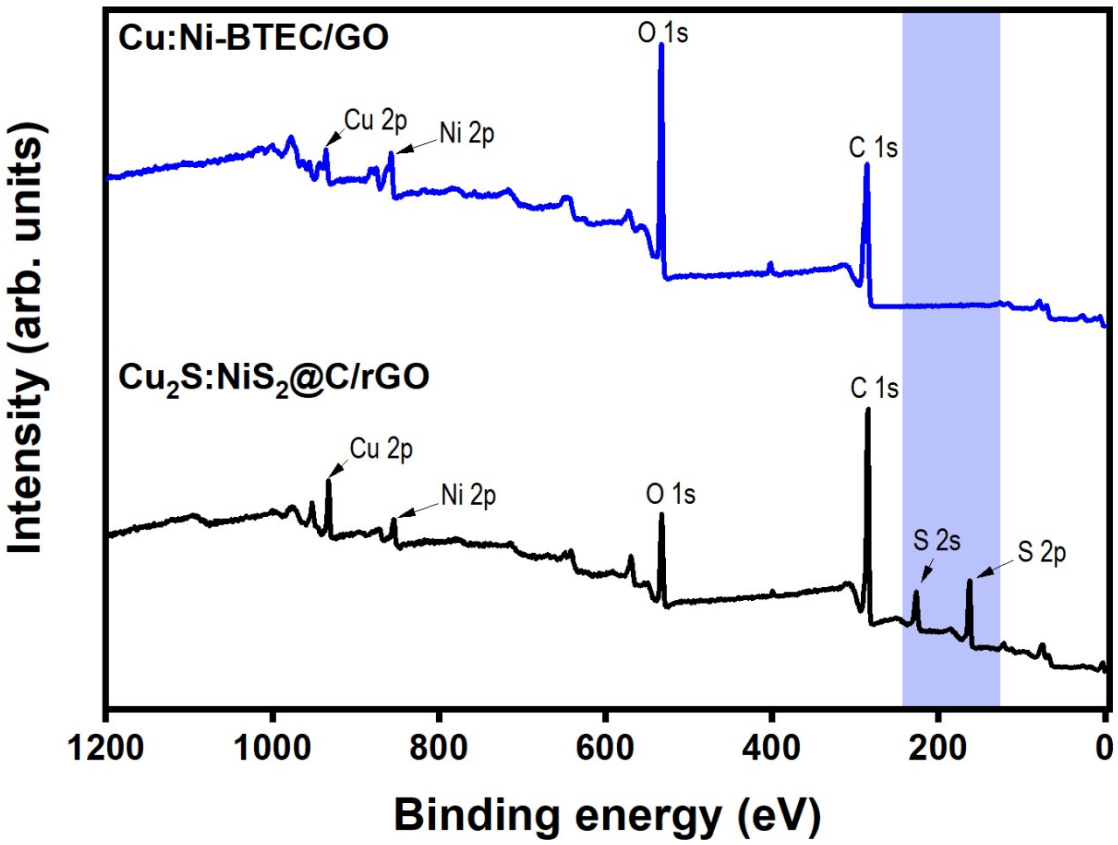

Figure. S4. XPS survey spectrum of Cu:Ni-BTEC/GO and Cu_2:NiS_2@C/rGO.

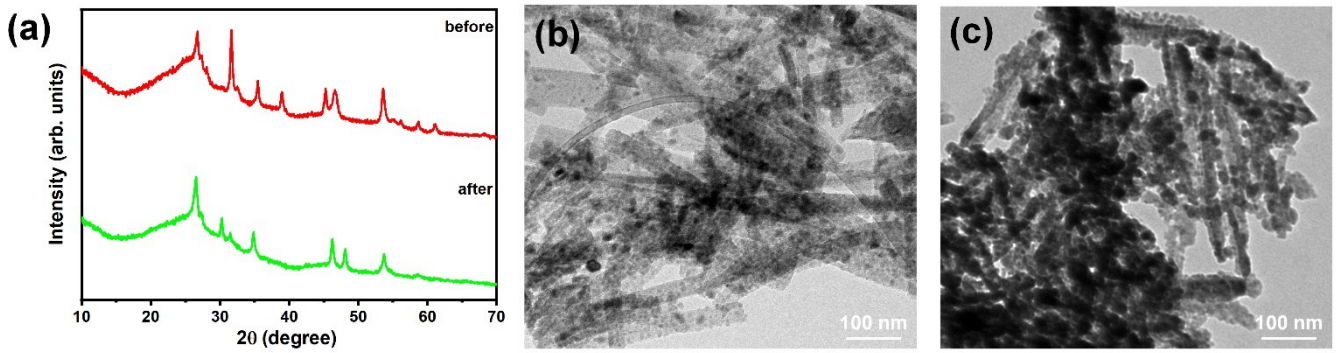

Figure. S5. (a) XRD patterns for reusability test of Cu_2S:NiS_2@C/rGO, TEM images of Cu_2S:NiS_2@C/rGO photocatalyst (b) before and (c) after 5th cycles.

Table S1. The wt.% of elemental analysis in the sample by ICP-OES.

Catalyst	Cu (wt.%)	RSD (%)	Ni (wt.%)	RSD (%)	S (wt.%)	RSD (%)
Cu_2S-NiS_2@C/rGO	21.2	1.26	17.8	2.18	14.8	0.94
Cu:Ni-BTEC/GO	13.4	1.79	11.5	1.99	-	-

Table S2. BET surface area, pore volume, and pore diameter of Cu:Ni-BTEC and its derivatives.

Catalyst	BET surface area (m^2 g^{-1})	Pore volume (cm^3 g^{-1})	Average pore size (nm)
Cu_2S:NiS_2@C/rGO	131	0.63	19
Cu:Ni-BTEC/GO	82	0.42	20
Cu-BTEC/GO	14	0.03	9
Ni-BTEC/GO	63	0.17	10
Cu:Ni-BTEC	62	0.32	20

The low surface area of Cu:Ni-BTEC is possibly due to the distortion molecule induced by the guest molecule/solvent filling the pore. Result in weak interaction of the framework with N_2 (low N_2 uptake) [1–3]. However, different MOFs with a relative low surface area were also reported, as shown in **Table S4**.

Table S3. The comparison study for Chan-Lam C-N coupling with other reported catalyst.

No	Catalyst	Structure	Condition	Additive	Light source	Nu. of exa.	Conv. (%)	Rec.(th)	Ref.
1	Cu_2S:NiS_2@C/rGO	core-shell;hybrid	1a (0.5 mmol), 1b (0.5 mmol), 5mg catalyst, MeOH:H_2O(3:1), 25°C, 6h, air	-	Xe-lamp (400-800 nm); 200 mW/cm^2	8, Other C-N oxidative coupling (6)	91-99	5	**This work**
2	Fe_3O_4@SiO_2/APTES/IMMPh@Ni^{2+} NPs	core-shell;hybrid	1a (1 mmol), 1b (2 mmol), 100mg catalyst, H_2O, 25-80°C, 1-6h	Na_3PO_4 (1 eq)	-	10	59-85	5	[4]
3	Fe_3O_4@SiO_2-dendrimer-encapsulated Cu(II)	core-shell;hybrid	1a (1.2 mmol), 1b (1 mmol), 10mg catalyst, MeOH, reflux (60-70°C), 1.5-6h	-	-	12	80-95	-	[5]
4	$Cu_3(BTC)_2$	Conventional	1a (0.3 mmol), 1b (0.3 mmol), 25mg catalyst, EtOH, 60°C, 12h, air	Et_3N (0.3 eq)	-	5	37-92	4	[6]
5	Cu_2S/TMEDA	-	1a (1 mmol), 1b (2 mmol), 34 mg catalyst, MeOH, r.t, 24-48, air	TMEDA (1eq)	-	14	60-90	-	[7]
6	Cu/grephene	Conventional	1a (1 mmol), 1b (1 mmol), 50 mg 5 wt% Cu catalyst, MeOH, 25°C, 1-6h, O_2	External O_2	Xe lamp	11	13-99	5	[8]

7	Polymer supported copper(II) complexes	-	1a (0.375 mmol), 1b (0.25 mmol), 10 mol % Cu(II) ions, EtOH, 70°C, 8h	Base K_2CO_3 (0.2 eq)	-	-	100	4	[9]
8	NiO NPs	Conventional	1a (1 mmol), 1b (1.5 mmol), 7mg catalyst, H_2O/EtOH (4:6), 50°C, 1-5	K_2CO_3 (2 eq)	-	9	70-83	6	[10]
9	Cu/g-C_3N_4	Conventional	1a (1 mmol), 1b (1 mmol), 140mg 20 mol% catalyst, MeOH, r.t-65°C, 8-12h, air	K_2CO_3 (1 eq)	blue LED (455–460 nm, 10 W)	19	56-95	6	[11]
10	N-enriched–GO/Cu	Conventional	1a (1 mmol), 1b (2 mmol), 2 mol% catalyst, EtOH:H_2O(1:1), 50-80°C, 1.5-5h, air	Base K_2CO_3 (2 eq)	-	16	40-98	5	[12]
11	*fac*-[Ir(ppy)$_3$]-assisted Cu^{II}	-	1a (0.38 mmol), 1b (0.25 mmol), 2 mol% catalyst, toluene:MeCN (1:1), 35°C, 20, air	2,6-lutidine (1 eq)	Blue LED	22	5-100	-	[13]
1a: arylboronic acid, 1b: aryl amine, entry 2-5 base on imidazole derivatives, entry 9-11 base on aniline derivatives									

Table S4. Comparison surface area of different MOF

No	MOF	Organic Linker	Morphology	Size* (nm)	BET surfaces area (m^2/g)	Ref.
1	Cu:Ni-BTEC	1,2,4,5-benzene-tetra-carboxylic acid	rod	32	62	This work
2	r-MIL-88A	fumaric acid	rod	100	24	[14]
	s-MIL-88A		Spindle	150	20	
	d-MIL-88A		Diamond	200	12	
3	Ni:Co-BDC	benzene-1,4-dicarboxylic acid	long-sheet	-	50	[15]
4	Co-BDC (MOF-71)	benzene-1,4-dicarboxylic acid	shale-shaped microcrystals	-	21	[16]
5	ZIF-L	2-methylimidazole	leaf-like	-	67	[17]
6	Mn-BDC	1,4-benzenedicarboxylic acid	laminar	5	5	[18]
7	MIL-88A	fumaric acid	hexagonal nanorod	400-600	15	[1]
	Ni-MIL-88A Ni/Fe(1:3)			400-600	37	
	Ni-MIL-88A Ni/Fe(3:1)			400-600	56	
8	MIL-53(Fe)	benzene-1,4-dicarboxylic acid	sheet	-	29	[19]
	MIL-53(Fe)-3H		spindle	2000	40	
	MIL-53(Fe)-5H		hexagonal spindle	3000	35	
	MIL-53(Fe)-10H		short columns	5000	30	
9	*a*MIL-88B a(amorphous)	terephthalic acid and 2-methylimidazole	spindle	90	60	[20]

*particles size base on width

Reference

[1] X.F. Lu, L. Yu, X.W. Lou, Highly crystalline Ni-doped FeP/carbon hollow nanorods as all-pH efficient and durable hydrogen evolving electrocatalysts, Sci. Adv. 5 (2019) eaav6009. doi:10.1126/sciadv.aav6009.

[2] L. Zhang, Y.H. Hu, Structure distortion of Zn4O13C24H 12 framework (MOF-5), Mater. Sci. Eng. B Solid-State Mater. Adv. Technol. 176 (2011) 573–578. doi:10.1016/j.mseb.2011.01.014.

[3] X. Liu, L. Zhang, J. Wang, Design strategies for MOF-derived porous functional materials: Preserving surfaces and nurturing pores, (2020). doi:10.1016/j.jmat.2020.10.008.

[4] M. Shahabi Nejad, N. Seyedi, H. Sheibani, S. Behzadi, Synthesis and characterization of Ni(II) complex functionalized silica-based magnetic nanocatalyst and its application in C–N and C–C cross-coupling reactions, Mol. Divers. 23 (2019) 527–539. doi:10.1007/s11030-018-9888-2.

[5] M. Esmaeilpour, A.R. Sardarian, H. Firouzabadi, Dendrimer-encapsulated Cu(Π) nanoparticles immobilized on superparamagnetic Fe $_3$ O $_4$ @SiO $_2$ nanoparticles as a novel recyclable catalyst for *N* -arylation of nitrogen heterocycles and green synthesis of

5-substituted 1 *H* -tetrazoles, Appl. Organomet. Chem. 32 (2018) e4300. doi:10.1002/aoc.4300.
[6] N. Anbu, A. Dhakshinamoorthy, Cu3(BTC)2 metal-organic framework catalyzed N-arylation of benzimidazoles and imidazoles with phenylboronic acid, J. Ind. Eng. Chem. 65 (2018) 120–126. doi:10.1016/j.jiec.2018.04.020.
[7] K. Janíková, L. Jedinák, T. Volná, P. Cankař, Chan-Lam cross-coupling reaction based on the Cu2S/TMEDA system, Tetrahedron. 74 (2018) 606–617. doi:10.1016/j.tet.2017.12.042.
[8] Y.L. Cui, X.N. Guo, Y.Y. Wang, X.Y. Guo, Visible-light-driven Photocatalytic N-arylation of Imidazole Derivatives and Arylboronic Acids on Cu/graphene catalyst, Sci. Rep. 5 (2015) 12005. doi:10.1038/srep12005.
[9] A. Bukowska, W. Bukowski, K. Bester, K. Hus, Polymer supported copper(II) amine-imine complexes in the C-N and A ^{3} coupling reactions, Appl. Organomet. Chem. 31 (2017) e3847. doi:10.1002/aoc.3847.
[10] T. Krishnaveni, K. Lakshmi, K. Kadirvelu, M. V. Kaveri, Exploration of Catalytic Activity of Quercetin Mediated Hydrothermally Synthesized NiO Nanoparticles Towards C–N Coupling of Nitrogen Heterocycles, Catal. Letters. 150 (2020) 1628–1640. doi:10.1007/s10562-019-03037-6.
[11] J.-Q. Di, M. Zhang, Y.-X. Chen, J.-X. Wang, S.-S. Geng, J.-Q. Tang, Z.-H. Zhang, Copper anchored on phosphorus g-C 3 N 4 as a highly efficient photocatalyst for the synthesis of N -arylpyridin-2-amines , Green Chem. 23 (2021) 1041–1049. doi:10.1039/d0gc03400b.
[12] N. Seyedi, M. Shahabi Nejad, K. Saidi, H. Sheibani, Fabrication of nitrogen-enriched graphene oxide/Cu NPs as a highly efficient and recyclable heterogeneous nanocatalyst for the Chan–Lam cross-coupling reaction, Appl. Organomet. Chem. 34 (2020) e5307. doi:10.1002/aoc.5307.
[13] W.-J. Yoo, T. Tsukamoto, S. Kobayashi, Visible-Light-Mediated Chan-Lam Coupling Reactions of Aryl Boronic Acids and Aniline Derivatives, Angew. Chemie Int. Ed. 54 (2015) 6587–6590. doi:10.1002/anie.201500074.
[14] X. Liao, F. Wang, F. Wang, Y. Cai, Y. Yao, B.T. Teng, Q. Hao, L. Shuxiang, Synthesis of (100) surface oriented MIL-88A-Fe with rod-like structure and its enhanced fenton-like performance for phenol removal, Appl. Catal. B Environ. 259 (2019) 118064. doi:10.1016/j.apcatb.2019.118064.
[15] J.F. Kurisingal, R. Babu, S.H. Kim, Y.X. Li, J.S. Chang, S.J. Cho, D.W. Park, Microwave-induced synthesis of a bimetallic charge-transfer metal organic framework: A promising host for the chemical fixation of CO2, Catal. Sci. Technol. 8 (2018) 591–600. doi:10.1039/c7cy02063e.
[16] X. Hu, H. Hu, C. Li, T. Li, X. Lou, Q. Chen, B. Hu, Cobalt-based metal organic framework with superior lithium anodic performance, J. Solid State Chem. 242 (2016) 71–76. doi:10.1016/j.jssc.2016.07.021.
[17] A.M. Nasir, N.A.H. Md Nordin, P.S. Goh, A.F. Ismail, Application of two-dimensional leaf-shaped zeolitic imidazolate framework (2D ZIF-L) as arsenite adsorbent: Kinetic, isotherm and mechanism, J. Mol. Liq. 250 (2018) 269–277. doi:10.1016/j.molliq.2017.12.005.
[18] H. Hu, X. Lou, C. Li, X. Hu, T. Li, Q. Chen, M. Shen, B. Hu, A thermally activated manganese 1,4-benzenedicarboxylate metal organic framework with high anodic capability for Li-ion batteries, New J. Chem. 40 (2016) 9746–9752. doi:10.1039/c6nj02179d.
[19] Y. Zhan, L. Shen, C. Xu, W. Zhao, Y. Cao, L. Jiang, MOF-derived porous Fe2O3 with controllable shapes and improved catalytic activities in H2S selective oxidation, CrystEngComm. 20 (2018) 3449–3454. doi:10.1039/c8ce00552d.
[20] C. Liu, J. Wang, J. Wan, Y. Cheng, R. Huang, C. Zhang, W. Hu, G. Wei, C. Yu, Amorphous Metal–Organic Framework-Dominated Nanocomposites with Both Compositional and

Structural Heterogeneity for Oxygen Evolution, Angew. Chemie Int. Ed. 59 (2020) 3630–3637. doi:10.1002/anie.201914587.